Flow Turbulence Combust (2009) 82:317–337
DOI 10.1007/s10494-008-9179-6

Turbulent Flow Produced by Piston Motion in a Spark-ignition Engine

V'yacheslav Akkerman · Mikhail Ivanov · Vitaly Bychkov

Received: 16 February 2007 / Accepted: 24 September 2008 / Published online: 5 November 2008

Abstract Turbulence produced by the piston motion in spark-ignition engines is studied by 2D axisymmetric numerical simulations in the cylindrical geometry as in the theoretical and experimental work by Breuer et al. (Flow Turbul Combust 74:145, 2005). The simulations are based on the Navier–Stokes gas-dynamic equations including viscosity, thermal conduction and non-slip at the walls. Piston motion is taken into account as a boundary condition. The turbulent flow is investigated for a wide range of the engine speed, 1,000–4,000 rpm, assuming both zero and non-zero initial turbulence. The turbulent rms-velocity and the integral length scale are investigated in axial and radial directions. The rms-turbulent velocity is typically an order-of-magnitude smaller than the piston speed. In the case of zero initial turbulence, the flow at the top-dead-center may be described as a combination of two large-scale vortex rings of a size determined by the engine geometry. When

V. Akkerman (✉) · M. Ivanov · V. Bychkov
Department of Physics, Umea University, 90187 Umea, Sweden
e-mail: akkerman@stanford.edu

V. Akkerman · M. Ivanov
Nuclear Safety Institute of Russian Academy of Sciences,
B. Tulskaya 52, 115191 Moscow, Russia

V. Akkerman · M. Ivanov
Department of Physics and Power Engineering,
Moscow Institute of Physics and Technology,
141700 Dolgoprudny, Moscow Region, Russia

Present Address:
V. Akkerman
Center for Turbulence Research,
Stanford University/NASA Ames Research Center,
488 Escondido Mall, Stanford, CA 94305-3035, USA

initial turbulence is strong, then the integral turbulent length demonstrates self-similar properties in a large range of crank angles. The results obtained agree with the experimental observations of Breuer et al. (Flow Turbul Combust 74:145, 2005).

Keywords Spark-ignition (SI) engine · Piston motion · Direct numerical simulations

1 Introduction

It is well-known that the burning rate of premixed turbulent flames depends strongly on the parameters of a turbulent flow [2–4]; combustion in spark-ignition (SI) engines is one of the most important examples. When turbulence is sufficiently strong, then the burning rate is controlled mainly by the turbulence parameters, rather than by thermo-chemical velocity of a planar laminar flame front. In that case, the most important parameter is the turbulent intensity measured by the root-mean-square (rms) flow velocity in one direction, $U_{\rm rms}$. A number of recent papers [5–16] demonstrated that the turbulent flame speed depends also on the integral turbulent length scale, on the turbulent spectrum and other particular features of the flow. For example, numerical simulations [8–10] suggested that the turbulent flame speed increases with the size of turbulent vortices Λ as $\Lambda^{2/3}$. Thus, one has to know quite well the parameters of the turbulent flow, which makes an inevitable and important step in the turbulent combustion research.

Concerning turbulence in SI-engines, an interesting recent paper [1] studied the integral turbulent length scale of the flow. Breuer et al. [1] pointed out that turbulence in an engine is essentially non-isotropic, which requires introducing at least two different integral length scales: one in the radial direction, Λ_r, and the other one along the axis of piston motion, Λ_z. The study in [1] was both theoretical and experimental. The theory was constructed under the assumption of axisymmetric turbulence and developed previous ideas and methods of [17, 18]. The measurements of [1] used technique similar to [19, 20]. Obviously, the theoretical approach of [1] is possible only for engine turbulence with negligible role of swirl and tumble (the basic concepts of a turbulent flow in an engine may be found, for example, in [21–23]).

Still, much has to be investigated about turbulence in engines even for an axisymmetric flow. Many questions remain open concerning not only the integral turbulent length scale, but even turbulent intensity, which is the basic flow parameter. For example, earlier $k-\varepsilon$ models of turbulence in engines suggested the rms-velocity comparable to the piston velocity (about 4–8 m/s for engine speed 2,000–3,000 rpm) [21]. However, these results are not consistent either with the general belief about turbulent flows [24] or with later studies of turbulence in engines [20]. For comparison, it is well-known that the rms-velocity of a statistically stationary turbulent flow in a cylindrical tube is an order of magnitude smaller than the average flow velocity, the factor is about 0.1–0.2, see [24] and references therein. One should expect a similar relation between the piston velocity and the rms-turbulent velocity in an engine with an ideally cylindrical combustion chamber as in [1], and with zero initial turbulence. Both in an engine and a tube, turbulence is produced in the

boundary layer because of the non-slip conditions at the walls. Taking the piston speed about 4–6 m/s, one evaluates the turbulent rms-velocity as 40 cm/s–1 m/s, which is comparable to the laminar normal speed of hydrocarbon flames. One finds similar experimental and numerical results for the rms-velocity in engines in [20]. According to [20], the turbulent intensity was rather high after the intake, up to (3–4) m/s, but it went noticeably down, to about (30–50) cm/s, as the piston approached the top-dead-centre (TDC). Turbulent intensity close to the TDC is of primary interest, since combustion happens mainly at that stage. The situation may be different for a more complicated engine geometry involving cavities in the combustion chamber and/or a complicated piston surface [23]. Still, in the present paper we considered the case of an ideally cylindrical chamber similar to the previous work [1]. To be rigorous, one has to investigate two intensities and two integral length scales for the axisymmetric flow: in the axial direction of compression, $U_{\mathrm{rms},z}$, Λ_z, and in the perpendicular radial direction, $U_{\mathrm{rms},r}$, Λ_r. We studied turbulence produced by the piston motion; turbulence at the intake is of minor interest for the present studies, but we have also taken it into account as initial conditions for the piston-produced flow.

The goal of the present paper is to investigate parameters of a turbulent flow in an SI-engine in the same cylindrical geometry as in [1]. For that purpose we performed 2D axisymmetric numerical simulations of the flow produced by the piston motion for the Navier–Stokes equations including viscosity, diffusion, thermal conduction and non-slip at the walls. Piston motion is taken into account as a boundary condition. Other physical parameters of the working gas correspond to the stoichiometric ethanol–air mixture, which is of great interest for the automotive industry [25]. We investigated the turbulent flow for a wide range of the engine speed, (1,000–4,000) rpm, which corresponds to the average piston velocities (2.66–10.66) m/s. In all cases we have obtained the turbulent rms-velocity an order of magnitude smaller than the piston speed. Besides, the rms-velocity in the direction of the piston motion is noticeably larger than in the radial direction. We also studied the integral turbulent length scales. In the case of zero initial turbulence, the flow at the TDC may be described as a combination of two large-scale non-symmetrical vortices: one close to the cylinder axis; the other one close to the walls. The characteristic size of the vortices is comparable to the chamber parameters. When initial turbulence is strong, the integral turbulent length demonstrates self-similar properties in a large range of crank angles. The simulations show that Λ_r varies a little during the piston motion; while Λ_z increases noticeably. The results obtained agree with the experimental observations of [1]. We should stress that some information remains beyond the 2D axisymmetric simulations, e.g. azimuthal fluctuations and stress component, as well as the tangential vortex stretching. As a result, the present studies may underestimate turbulence generated by the piston motion, which makes comparison to 3D experiments rather qualitative than quantitative. Meanwhile, the present 2D simulations give the basic qualitative idea about a piston-generated flow in an SI-engine. The role of azimuthal fluctuations and stress component, and tangential vortex stretching will be considered elsewhere.

The present paper is organized as follows: in Section 2 we describe the basic equations used in direct numerical simulations and present main parameters of the problem; in Section 3 the simulation results are discussed; we conclude the paper with a brief summary.

2 Basic Equations and the Numerical Method

A 2D axisymmetric flow in an engine is described by the following set of equations

$$\frac{\partial}{\partial t}\rho + \frac{\partial}{\partial x_i}(\rho\, u_i) = 0, \tag{1}$$

$$\frac{\partial}{\partial t}(\rho\, u_i) + \frac{\partial}{\partial x_j}\left(\rho\, u_i u_j + \delta_{i,j} P\right) - \gamma_{i,j} = 0, \tag{2}$$

$$\frac{\partial}{\partial t}\left(\rho\varepsilon + \frac{1}{2}\rho\, u_i u_j\right) + \frac{\partial}{\partial x_i}\left(\rho\, u_i h + \frac{1}{2}\rho\, u_i u_j u_j + q_i - u_j \gamma_{i,j}\right) = 0, \tag{3}$$

where u_i are the velocity components, $\varepsilon = C_V T$ is the internal energy, $h = \varepsilon + P/\rho$ is the enthalpy, C_V is the heat capacity per unit mass at constant volume, which was calculated as

$$C_V = \left(\sum_i \frac{Y_i}{M_i} C_{Vi}\right)\left(\sum_i \frac{Y_i}{M_i}\right)^{-1}. \tag{4}$$

Here Y_i is the mass fraction of a substance i in the gas mixture, M_i and C_{Vi} are the respective molecular mass and heat capacity at constant volume. Basically, the present problem may be studied even for a homogeneous perfect gas. We used a stoichiometric ethanol–air mixture as a working gas because of increased interest to ethanol burning in automotive industry [25]. Total pressure is determined by the perfect gas law

$$P = \left(\sum_i \frac{Y_i}{M_i}\right) R_g \rho\, T, \tag{5}$$

where $R_g \approx 8.31\ \mathrm{J}/(\mathrm{mol}\cdot\mathrm{K})$ is the perfect gas constant. The stress tensor $\gamma_{i,j}$ is given by

$$\gamma_{i,j} = \mu\left(\frac{\partial u_i}{\partial x_j} + \frac{\partial u_j}{\partial x_i} - \frac{2}{3}\frac{\partial u_k}{\partial x_k}\delta_{i,j}\right), \tag{6}$$

and the energy diffusion vector q_i is

$$q_i = -\mu\frac{C_P}{\mathrm{Pr}}\frac{\partial T}{\partial x_i}. \tag{7}$$

Here μ is the dynamic viscosity, $C_P = C_V + R_g$ is the total heat capacity per unit mass at constant pressure, and Pr is the Prandtl number. Similar to [26], we chose $\mathrm{Pr} = 0.7$ and calculated the dynamic viscosity as

$$\mu = \sum_i \alpha_i \mu_i \left(\sum \alpha_j \Phi_{i,j}\right)^{-1}, \tag{8}$$

where α_i and μ_i are the molar fraction and viscosity of substance i; the factor $\Phi_{i,j}$ is calculated as

$$\Phi_{i,j} = \frac{1}{2\sqrt{2}}\left[1 + \left(\frac{\mu_i}{\mu_j}\right)^{1/2}\left(\frac{M_j}{M_i}\right)^{1/4}\right]^2\left(1 + \frac{M_i}{M_j}\right)^{-1/2}. \tag{9}$$

The viscosity coefficients for different substances are tabulated in [26–28].

In the simulations we used the numerical method of "large particles" (Belotserkovsky method), see [29, 30] for details. The main idea of the method is to separate the Lagrangian and Eulerian terms in the hydrodynamic equations. As a result, the mixture is replaced by a set of "large particles", which coincide with the Eulerian grid cells at any time instant. Every time step is divided into tree different sub-steps. At the first (Eulerian) sub-step, the "large particles" are assumed to be fixed in space; thus we calculate the change in hydrodynamic parameters on the fixed Eulerian space-grid neglecting mass, momentum and energy transfer. An explicit scheme is used for that purpose. At the second (Lagrangian) sub-step, the obtained hydrodynamic values are used to find transfer through the cell boundaries. Finally, at the third sub-step, we recalculate all hydrodynamic parameters for every cell and for the whole flow. Diffusion and thermal conduction are calculated at the last stage, while energy transfer is calculated partially at the first sub-step, and partially at the third one. The described procedure leads to high stability of the method, which allows solving various hydrodynamic problems. A detailed description of the method is available in [30]; basic elements of the method were presented in [31]. Since that time, the method was used in investigations of turbulent wakes, the Rayleigh–Taylor instability, Taylor–Couette turbulence, astrophysical turbulence in accretion disks and Supernovae, and other phenomena [30]. In combustion science this method (and this particular code) was used successfully in predicting knock in SI-engines [32].

Geometry of a combustion chamber was taken similar to [1]. We considered a cylindrical chamber with the radius (half-bore) $R = 40$ mm and stroke $L = 80$ mm. The height of the chamber at maximal compression (clearance) is $H = 10.6$ mm, the compression ratio is $r_c = 1 + L/H \approx 8.5$, and the crank shaft ratio is $a = 0.29$. Then the instantaneous piston position is given by [26]

$$h(\theta) = H + \frac{L}{2}\left(1 + \cos\theta + \frac{1}{a}\left[\sqrt{1 - a^2\sin^2\theta} - 1\right]\right), \tag{10}$$

and the piston velocity is

$$U_p = U_{p0}\frac{\pi}{2}\left(1 + \frac{a\cos\theta}{\sqrt{1 - a^2\sin^2\theta}}\right)\sin\theta, \tag{11}$$

where θ is the crank angle. The average piston velocity is related to the frequency as $U_{p0} = L\omega/\pi$ (or $U_{p0} = 2LN/60$, if the engine speed N is measured in rpm). We used the engine speed 1,000, 2,000, 4,000 (rpm) in the present simulations. Figure 1 shows the scaled piston position h/h_{BDC} (the solid line) and the scaled velocity

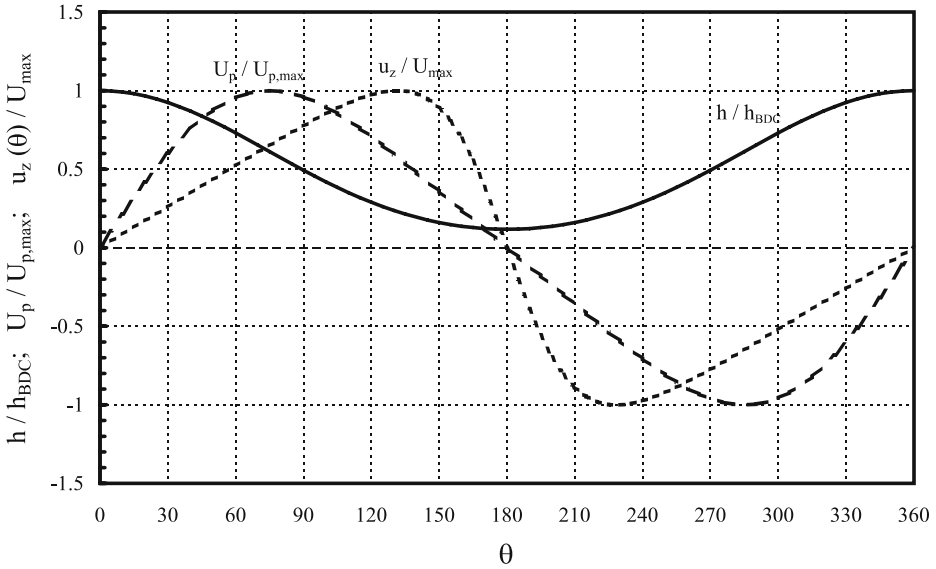

Fig. 1 The scaled piston position h/h_{BDC} (*solid*) and the scaled velocity $U_p/U_{p,\max}$(*dashed*) versus the crank angle θ. The dotted line shows $u_z/u_{z,\max}$, where $u_{z,\max}$ is calculated for a fixed position z

$U_p/U_{p,\max}$ (the dashed line) versus the crank angle. Zero angle $\theta = 0°$ corresponds to minimal gas compression at the bottom-dead-centre (BDC) at maximal $h_{\mathrm{BDC}} = H + L$. Maximal compression is achieved at the TDC with $h_{\mathrm{TDC}} = H$, $\theta = 180°$. The piston velocity reaches the maximal value $U_{p,\max}/U_{p0} \approx 1.64$ at $\theta \approx 75°$. The dotted plot of Fig. 1 will be discussed later.

To reduce the computational time, we considered an axisymmetric flow in a cylindrical chamber. We stress that the 2D axisymmetric flow is not quite the same as the flow studied in [1], which possessed a 3D instantaneous velocity field with axisymmetric statistical properties. In the 2D simulations, we miss, for example, azimuthal velocity fluctuations and stress component, and tangential vortex stretching. Still, as we demonstrate below, the simplified 2D axisymmetric geometry reproduces the main results of [1] quite well. Azimuthal fluctuations and stress will be studied in a separate 3D numerical work. We used adiabatic and non-slip boundary conditions at the walls

$$\mathbf{u} = 0, \tag{12}$$

$$\hat{\mathbf{n}} \cdot \nabla T = 0, \tag{13}$$

where $\hat{\mathbf{n}}$ is a normal vector at the wall. Initially, at $\theta = 0°$, we had pressure $P_0 = 10^5$ Pa and temperature $T_0 = 300$ K. We studied the cases of both zero and non-zero initial turbulence. Simulations were performed only for the compression stage of piston motion ($0° < \theta < 180°$). We used a uniform square grid with the grid walls parallel to the coordinate axes, and with the grid size $\Delta \approx 0.18$ mm in both directions, which corresponds to 220 cells in the radial direction and 498 cells in the z-direction

at the BDC instant. Total number of the grid cells was about 1.1×10^5 at the BDC instant; the grid size remained the same during the simulation runs. The important question is if the length scale of energy dissipations Λ_ν may be resolved with such a grid. In the present work we considered 2D axisymmetric turbulence, which cannot be described by the Kolmogorov spectrum. Still, as an order-of-magnitude estimation, we can take the length scale Λ_ν, which is related to the integral length scale Λ as $\Lambda_\nu \propto Re_{turb}^{-3/4} \Lambda$. The characteristic value of the Reynolds number Re based on the cylinder radius and the average piston velocity is about 10^4. However, the definition for $\mathrm{Re}_{\mathrm{turb}}$ employs U_{rms} and Λ as the scales of velocity and length [33], which leads to noticeably smaller values of Re. For example, in the case of zero initial turbulence, U_{rms} is an order of magnitude smaller than the average piston velocity, while the vortex size is determined by the clearance. Then $\mathrm{Re}_{\mathrm{turb}} \approx 10^3$, and the length scale of dissipations is about $\Lambda_\nu \propto \Lambda/180$, which is comparable to the cell size in the present simulations. Besides, recent studies of turbulence in different configurations demonstrated that practically the whole turbulent energy is stored in large scale vortices [29, 30]. As a result, performing the simulations, one has to take care mainly of the large-scale vortices as the main energy carriers. There is also another important reason, why one may be satisfied with resolution of the present paper. The present study has been performed keeping in mind turbulent combustion in an engine. Recent numerical and experimental works on turbulent burning demonstrated that only large-scale vortices are important for flame propagation [13, 15, 16, 34]. It was obtained experimentally and demonstrated theoretically that the inner cut-off of turbulent flame wrinkles is well-correlated with the cut-off of the Darrieus–Landau instability, Λ_c. The latter is typically 1–2 orders of magnitude larger than the formal mathematical definition for the flame thickness $L_f \equiv \nu/\mathrm{Pr}\, U_f$. This result should not be interpreted as a dominant influence of the instability in turbulent combustion. In a certain sense, the Darrieus–Landau cut-off works as an effective flame thickness. The cut-off indicates when a hydrodynamic flow (turbulent or laminar) becomes influenced strongly by thermal conduction. The Darrieus–Landau cut-off for typical hydrocarbon flames is about $\Lambda_c = (0.2 - 0.6)$ cm [13]. These values are much larger than the cell size in the present simulations. For this reason, present simulations resolve quite well all turbulent length scales important for burning.

It was pointed out in [1] that turbulence in an engine is strongly anisotropic, and there is no single integral turbulent length in the flow. Even assuming axial symmetry, one needs two length scales and two turbulent rms-velocities to describe the flow. The instantaneous rms-velocities are given by

$$U_{\mathrm{rms},i}^2(\theta) = \left\langle \tilde{u}_i^2(r, z, \theta) \right\rangle, \tag{14}$$

where

$$\tilde{u}_i(\theta) = u_i(r, z, \theta) - \langle u_i(r, z, \theta) \rangle \tag{15}$$

is the velocity deviation from the instantaneous average value (index i denotes r or z). Similar to [1], we calculated the integral length scales in r and z directions as

$$\Lambda_i(\theta) = \frac{3}{4} \frac{1}{U_{\mathrm{rms}}^2} \iint_V R_i(r, z, \theta) \frac{r\, dr\, dz}{r^2 + z^2}, \tag{16}$$

where

$$R_i(r, z, \theta) = \left\langle \tilde{u}_i(r_1, z_1, \theta)\, \tilde{u}_i(r_1 + r,\ z_1 + z,\ \theta) \right\rangle_{r_1, z_1} \tag{17}$$

is the velocity correlation between the points (r, z) and $(r_1 + r_2, z_1 + z_2)$, see [1] for details. In the limit of zero separation ($r = z = 0$), the correlation function (17) is reduced to the square of the rms-velocity in i- direction, (14).

3 Results and Discussion

We investigated dynamics of a gas compressed by the piston motion in a cylindrical SI-engine. First, we considered the case of no initial turbulence, when the gas was initially at rest. In that case the flow is generated by the piston motion only. Assuming ideally slip walls, one can obtain an analytical 1D compression flow in that case

$$\rho(t) = \rho_0 \frac{h_0}{h(t)}, \quad u_z = -\frac{U_p(t)}{h(t)} z, \tag{18}$$

where the piston velocity is determined by (10), and time is related to the crank angle as $\theta = \omega t$ (or $\theta = \pi\, N\, t/30$ with N in rpm). Figure 2 compares the 1D flow given by (18) (the solid line) to the z-velocity component averaged over radial coordinate at different time instants (the dotted line). To be particular, for comparison we have chosen the distance $z = H$ from the cylinder bottom, which coincides with the clearance and with the border of the observation window in the experiments [1]. The

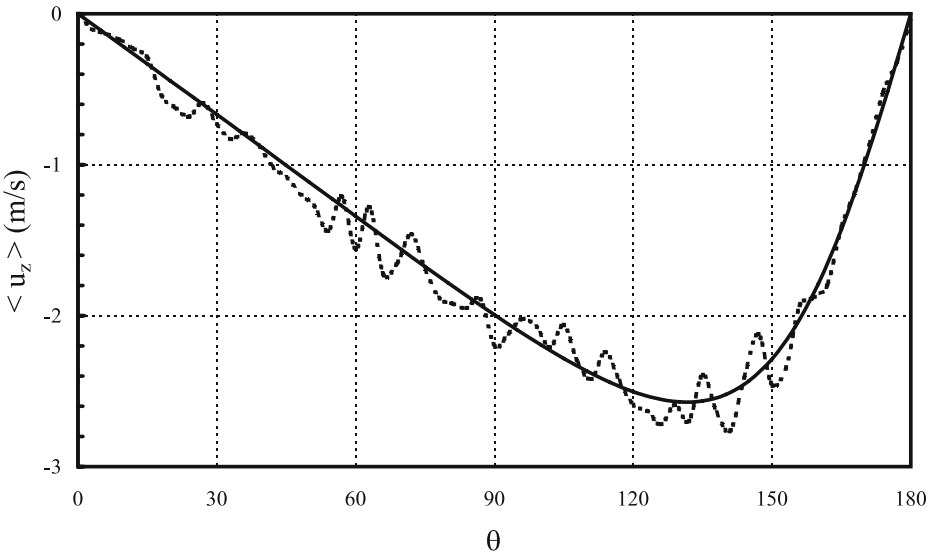

Fig. 2 The velocity of a 1D compression flow, (18), (*solid*) and the averaged z-velocity in the numerical simulations (*dotted*) for $z = H$ versus the crank angle θ

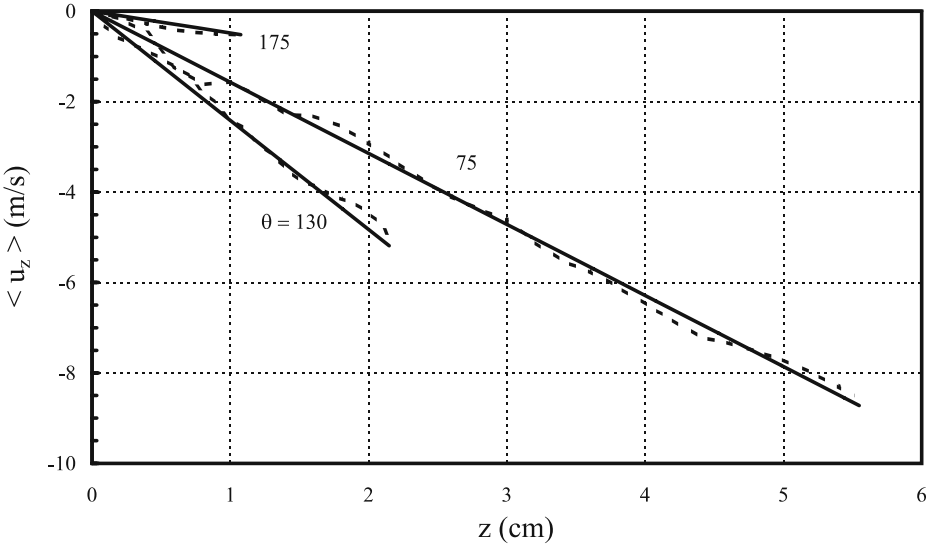

Fig. 3 The z-velocity versus the z-coordinate for the different crank angles $\theta = 75°; 130°; 175°$: the 1D analytical solution, (18), (*solid*) and the averaged numerical results (*dotted*)

analytical formula agrees quite well with the numerical simulations. Figure 3 presents the dependence of the averaged z-velocity versus the z-coordinate for different crank angles $\theta = 75°; 130°; 175°$. Similar to Fig. 2, the solid lines in Fig. 3 present the analytical solution (18), while the averaged numerical results are shown by the dotted lines. Again, one can see good agreement between the dotted and the solid plots. Still, the realistic non-slip boundary conditions make the flow (18) non-uniform, induce r-velocity component, and generate vorticity and turbulence. Figure 4 demonstrates the turbulent rms-velocity in different directions $U_{\mathrm{rms},z}$ (Fig. 4a) and $U_{\mathrm{rms},r}$ (Fig. 4b) versus the crank angle for $N = 1,000$; 2,000; 3,000 rpm. The solid lines show the rms-velocities averaged over the whole gas volume, which is the most natural way of averaging. However, the experimental installation in [1] allowed measuring turbulent parameters only in space corresponding to the clearance. For this reason, Fig. 4 presents also rms-velocities averaged over the clearance only. These dotted plots underestimate noticeably all rms-velocities at the beginning of the piston motion, which indicates that the turbulence distribution in space is not uniform. Close to the TDC, both solid and dotted curves come together, since both regions of averaging coincide in that case. According to Fig. 4a, the turbulence intensity changes with the crank angle in a similar way for different engine speeds. At the beginning, the turbulent intensity increases to a maximum achieved at $\theta \approx 90°$–$110°$; then it goes down to a much smaller value at the TDC. The curves in Fig. 4 resemble qualitatively the plot for the piston velocity in Fig. 1, but the maximum of the rms-velocity is delayed in time in comparison with the maximal piston velocity achieved at $\theta \approx 75°$. In order to understand this delay, we considered the analytical formula for u_z, Eq. (18), in the case of slip walls. Choosing any fixed position z, we calculated the maximal u_z designated by $u_{z,\max}$. This value corresponds, obviously, to the maximum of $U_p(t)/h(t)$, which is achieved at $\theta \approx 130°$ and which is delayed with respect to

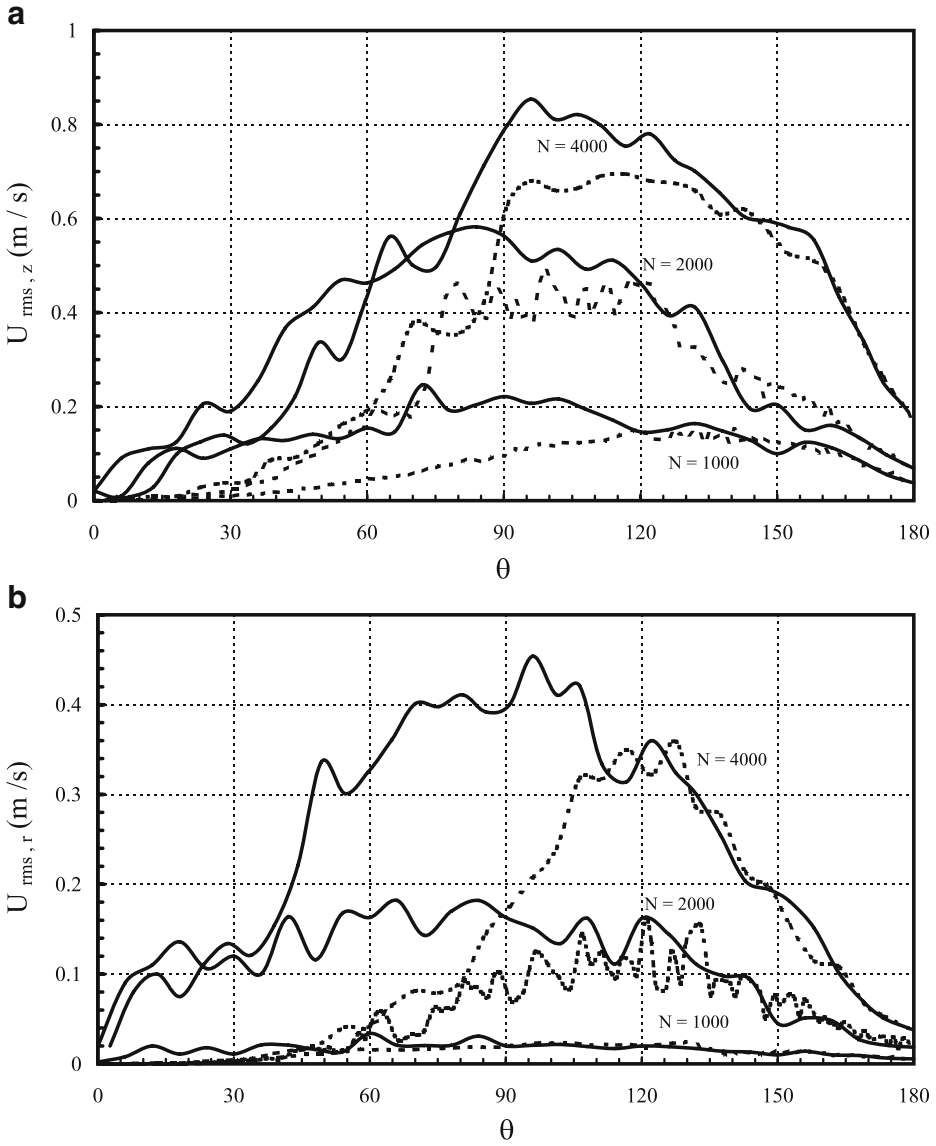

Fig. 4 The turbulent rms-velocity in different directions, $U_{\mathrm{rms},z}$ (**a**) and $U_{\mathrm{rms},r}$ (**b**), versus the crank angle θ for different engine speeds: $N = 1,000, 2,000, 4,000$ rpm. Averaging was performed over the whole flow (*solid*) and over the clearance only (*dotted*)

the maximum of the piston velocity. The dotted line in Fig. 1 presents $u_z/u_{z,\max}$ according to Eq. (18). The delay in the maximal turbulent intensity in comparison with the maximal piston velocity is correlated with the delay of $u_{z,\max}$. Another important point is that the rms-turbulent velocity is an order of magnitude smaller than the average piston speed. The average piston speed equals 2.6 m/s, 5.3 m/s, 10.6 m/s

for 1,000, 2,000, 4,000 rpm, while the respective rms-velocity in z-direction is about 0.25 m/s, 0.58 m/s, 0.85 m/s. Thus in the case of moderate engine speed, 1,000–2,000 rpm, the rms-velocity becomes comparable to the planar flame speed, U_f, which is an important conclusion for turbulent combustion research. Besides, $U_{\mathrm{rms},z}$ is noticeably larger than $U_{\mathrm{rms},r}$. For example, in the case of 2,000 rpm, their maximal values are $U_{\mathrm{rms},z} \approx 58$ *cm/s* and $U_{\mathrm{rms},r} \approx 18$ *cm/s*. Thus the "axial" turbulence dominates over the "radial" one. Figure 5 shows the integral turbulent length scales Λ_z (solid) and Λ_r (dotted) versus the crank angle θ for $N = 2,000$ rpm. These parameters were calculated using (16, 17). Time dependence of Λ_z exhibits strong irregular pulsations between 2 cm and 4 cm, with slightly higher maxima close to the beginning (around $\theta = 20° - 40°$) and the end (at $\theta \approx 170°$). Finally, at the TDC, at $\theta \approx 180°$, the value of Λ_z goes down to 1.17 cm, which is obviously determined by clearance. On the contrary, Λ_r experiences weak pulsations during the piston motion, since radius of the cylinder does not change. Most of the time, Λ_r is about 0.8–0.9 cm, but it goes up to 1.87 cm at the TDC, which is roughly 1/2 of the cylinder radius.

In order to understand spatial distribution of turbulence in an engine, Fig. 6 shows the vorticity distribution at the different crank angles $\theta = 60°$; 120°; 170°; 180° (Fig. 6a–d, respectively). Black solid lines present streamlines of the flow. The "half-dark" corresponds to clockwise rotation (negative), while counterclockwise rotation (positive) is shown by dark; vorticity is almost zero in the light regions. There is almost no turbulence in Fig. 6a at $\theta = 60°$ and the streamlines are plane-parallel except for the very bottom of the cylinder, where the analytical compression velocity of (18) goes to zero. Turbulence becomes better pronounced in Fig. 6b at $\theta = 120°$. In that case, one can see a well-determined dark region of counterclockwise vorticity along the wall. The region is non-symmetric; it is strongly shifted to the piston, where plane-parallel velocity is higher. The vorticity distribution indicates a

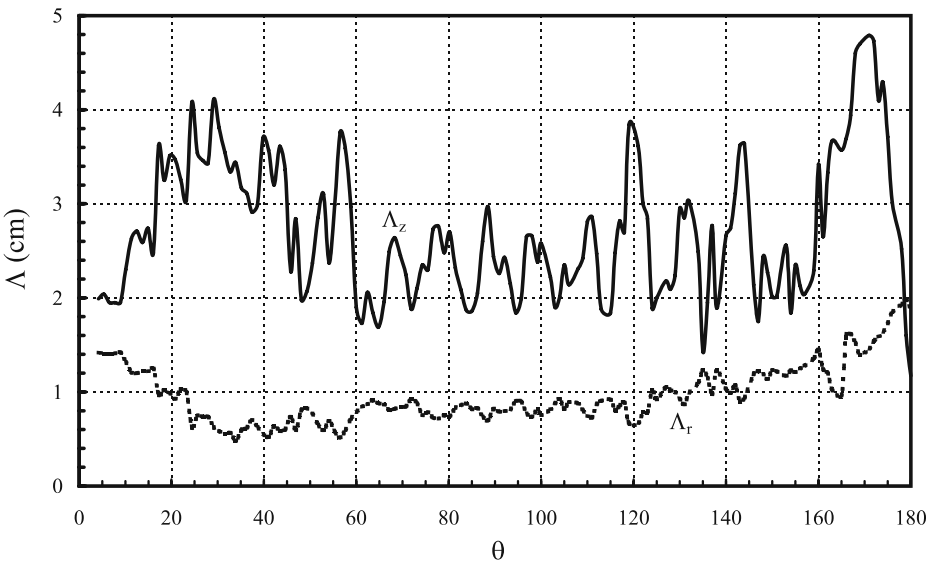

Fig. 5 The integral turbulent length scales, Λ_z (*solid*) and Λ_r (*dotted*), versus the crank angle θ for the engine speed $N = 2,000$ rpm

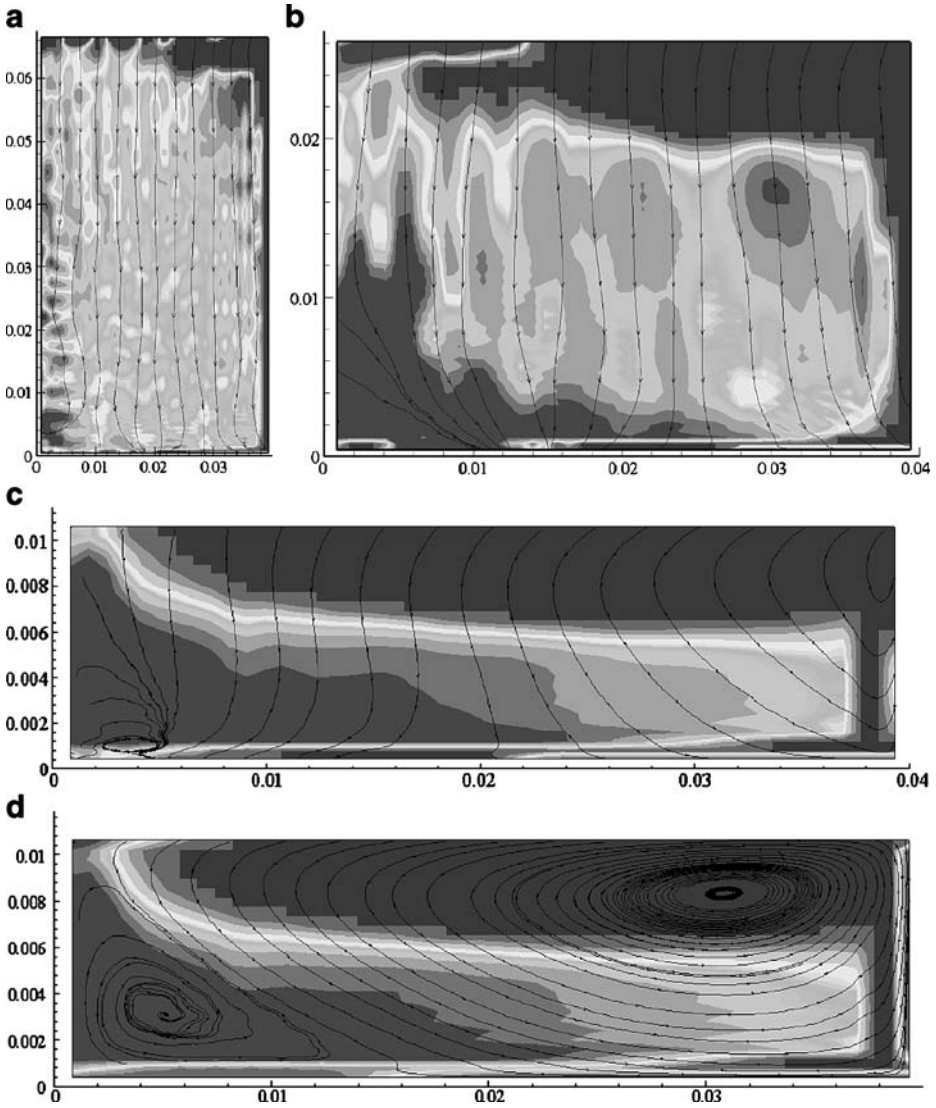

Fig. 6 The snapshots of vorticity in the case of zero initial turbulence at different crank angles $\theta = 60°; 120°; 170°; 180°$ (**a**–**d**). The "half-dark" corresponds to clockwise rotation (negative), while counterclockwise rotation (positive) is shown by dark; vorticity is almost zero in the light regions. *Black solid lines* present streamlines of the flow

boundary layer along the wall, which works as the main source of turbulence. At the same time, the "half-dark" region of vorticity of the opposite direction is formed at the cylinder axis close to the bottom. Streamlines in Fig. 6b are still mostly plane-parallel, which indicates that quasi plane-parallel compression, (18), dominates in the flow. Figures 6c, d present vorticity close to the piston stop at the TDC. In those cases, regions of noticeable vorticity fill practically the whole cylinder volume. Vorticity

is strongly correlated into two regions of clockwise and counterclockwise rotation. These regions become pronounced in the streamlines in Fig. 6d at the TDC: we can see two well-correlated vortices in the figure. Keeping in mind the axisymmetric structure, these two vortices correspond to a couple of vortex rings dominating in the flow. The vortex size in Fig. 6d obviously correlates with the integral length scales presented above, $\Lambda_r = 1.87$ cm, $\Lambda_z = 1.17$ cm. Thus, in the case of zero initial turbulence, the piston motion leads to well-correlated vortices with sizes determined by the engine geometry. The turbulent intensity is approximately proportional to the average piston speed. At the same time, it is an order of magnitude smaller than the piston velocity, which makes it comparable to the laminar speed of planar hydrocarbon flames.

It is also interesting to compare the present simulations to the results of [1]. Compression in [1] started with quite strong initial turbulence. In scope of the theoretical model [1], initial turbulence was assumed to be uniform $U^2_{\mathrm{rms},z} = U^2_{\mathrm{rms},r} = 13.3\ \mathrm{m}^2/\mathrm{s}^2$ and isotropic, with the integral length scales $\Lambda_{r,0} = \Lambda_{z,0} = 0.3$ mm. The experiments [1] demonstrated larger initial integral length scales, about $\Lambda_{r,0} \approx$ (0.5–0.7) mm, $\Lambda_{z,0} \approx$ (0.7–1) mm, though they were comparable by an order of magnitude to the theoretical assumptions. Unfortunately, we cannot resolve such small-scale turbulence in the present simulations, since the numerical cell size would be about the integral length scales in that case. Besides, such small vortices play a minor role for flame propagation. Flame wrinkles of this size are strongly smoothed by thermal conduction because of a rather large effective finite flame thickness discussed above, see also [13, 15]. For this reason, we used initial turbulence as strong as in [1], but with larger initial integral length scale $\Lambda_{z,0} = \Lambda_{r,0} = 1$ cm, see Fig. 7a. Similar to [1], the calculations were performed for the engine speed $N = 2,000$ rpm. The vorticity distribution in that case is presented in Fig. 7 for the crank angles 0; 60; 75; 132; 180 (Fig. 7a–e, respectively). Similar to Fig. 6, the "half-dark" corresponds to clockwise rotation (negative), while counterclockwise rotation (positive) is shown by dark; vorticity is almost zero in the light regions. Black solid lines present streamlines of the flow. Figure 7a shows the initial distribution of vorticity. Figure 7b demonstrates more or less the same pattern of vortices at $\theta = 60°$ of sizes close to the initial ones, but the pattern is less regular and the streamlines are obviously dominated by the quasi-1D compression motion. At $\theta = 75°$, 132° (Fig. 7c, d), vortices become irregular; they are noticeably larger in size than the original ones of Fig. 7a. Finally, as shown in Fig. 7e, the distribution of vorticity at the TDC has many common features with Fig. 6d: we observe an organized vortex ring at the cylinder wall shifted to the piston, and a half-dark region of clockwise vorticity close to the axis. However, this time the clockwise vortex is less pronounced. Figures 8, 9 present the quantitative characteristics of the flow. The solid lines represent averaging over the whole chamber, while the dotted/dashed lines are related to averaging only over the volume observed experimentally in Ref. [1]. According to Fig. 8, the rms-velocity goes down fast in comparison with the large initial values; it reaches a local minimum in z-direction close to $\theta = 50°$ and a local minimum in r-direction close to $\theta = 70°$ (though the minima are quite shallow). As for the values averaged over the volume observed experimentally in Ref. [1], it is interesting that a minimum for $U_{\mathrm{rms},z}$ is hardly seen, and there is no any minimum at all for $U_{\mathrm{rms},r}$. It means that minima cannot be observed experimentally through a window of the setup [1]. Then rms-velocities start increasing again, and attain a

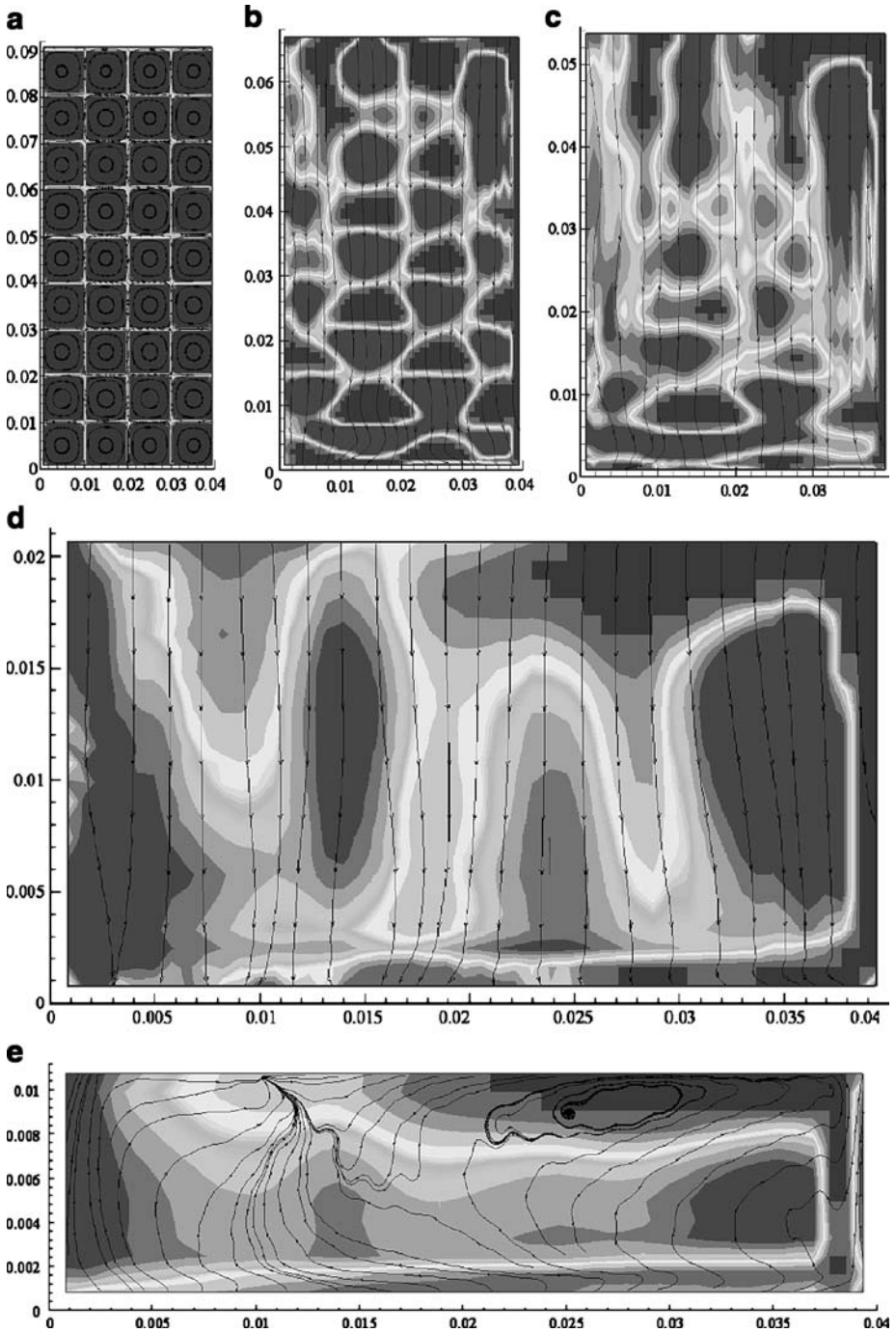

Fig. 7 The snapshots of vorticity in the case of non-zero initial turbulence at different crank angles $\theta = 0°; 60°; 78°; 132°; 180°$ (**a**–**e**). The "half-dark" corresponds to clockwise rotation (negative), while counterclockwise rotation (positive) is shown by dark; vorticity is almost zero in the light regions. *Black solid lines* present streamlines of the flow

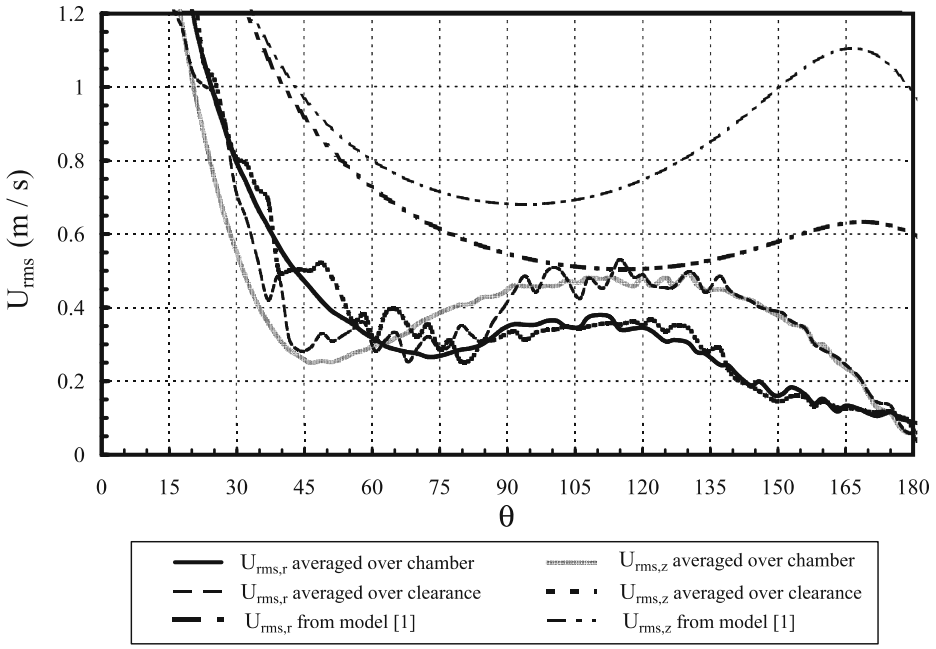

Fig. 8 The turbulent rms-velocities in different directions, $U_{\mathrm{rms},z}$ and $U_{\mathrm{rms},r}$, versus the crank angle θ for the engine speed $N = 2,000$ rpm and non-zero initial turbulence. The averaging was performed over the whole flow and over the clearance only. The model result of Ref. [1] calculated from Reynolds stress is also shown in the plot

local maximum somewhere between $\theta = 90°$ and $\theta = 130°$. The maximum is rather flat and it correlates well with the maxima of the piston velocity and the 1D z-velocity (see Fig. 1). The turbulent intensity goes down again as the piston stops at the TDC. The dashed-dotted lines of Fig. 8 show the results of the model of Ref. [1] calculated from Reynolds stress. We can see qualitative agreement of the present simulations with the model, though the results differ quantitatively. It is possible that such a quantitative difference happens because of the limitations of the present 2D axisymmetric modeling (in particular, due to missing of the tangential vortex stretching, etc). Unfortunately, Ref. [1] did not report experimental data for the Reynolds stress. The simulation results agree also qualitatively with the experimental measurements of the rms-velocity of Ref. [20] in spite of different geometrical parameters of the engine cylinder. For turbulent combustion studies, the most interesting values of rms-velocity are those at $\theta > 130°$. The characteristic rms-velocities of Fig. 8 at these angles are close to the respective values of Fig. 4 obtained for zero initial turbulence; namely, $U_{\mathrm{rms},z} \approx 50$ cm/s, $U_{\mathrm{rms},r} \approx 38$ cm/s. These values are comparable to the planar flame velocity.

Figure 9a shows the integral turbulent length scales in z- and r-directions (solid and dotted lines, respectively. The value Λ_r varies a little during gas compression, and remains close to 1 cm all the time. In contrast, Λ_z decreases at the beginning of compression, reaches minimum of about 0.5 cm close to $\theta = 50°$, then increases again up to 2–2.5 cm close to $\theta = 120° - 150°$, and goes abruptly down to 1 cm at

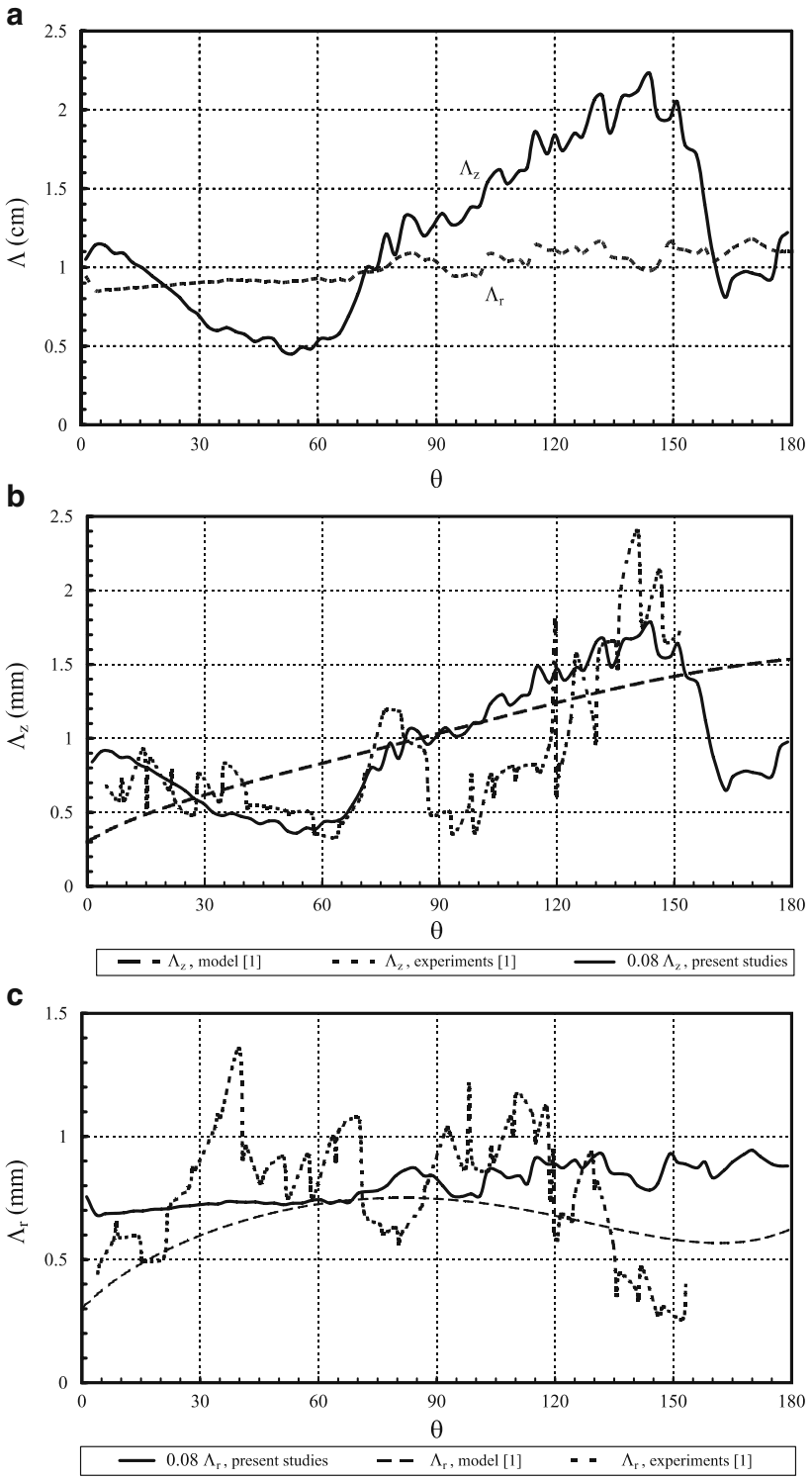
a
Λ (cm)
Λz
Λr
θ
b
Λz (mm)
θ
Λz, model [1]
Λz, experiments [1]
0.08 Λz, present studies
c
Λr (mm)
θ
0.08 Λr, present studies
Λr, model [1]
Λr, experiments [1]

◀ **Fig. 9** The integral turbulent length scale in different directions, Λ_z (*solid*) and Λ_r (*dotted*), versus the crank angle θ for the engine speed $N = 2,000$ rpm and non-zero initial turbulence (plot **a**). Plots (**b**) and (**c**) compare present results (rescaled by initial values) to the experimental data and the dole of Ref. [1]

the TDC. First, we point out that the maxima and minima of Λ_z correlate well with the maxima and minima of $U_{\mathrm{rms},z}$. Second, they correlate well with the experiments of Ref. [1], though this correlation is concealed by different initial values. As we

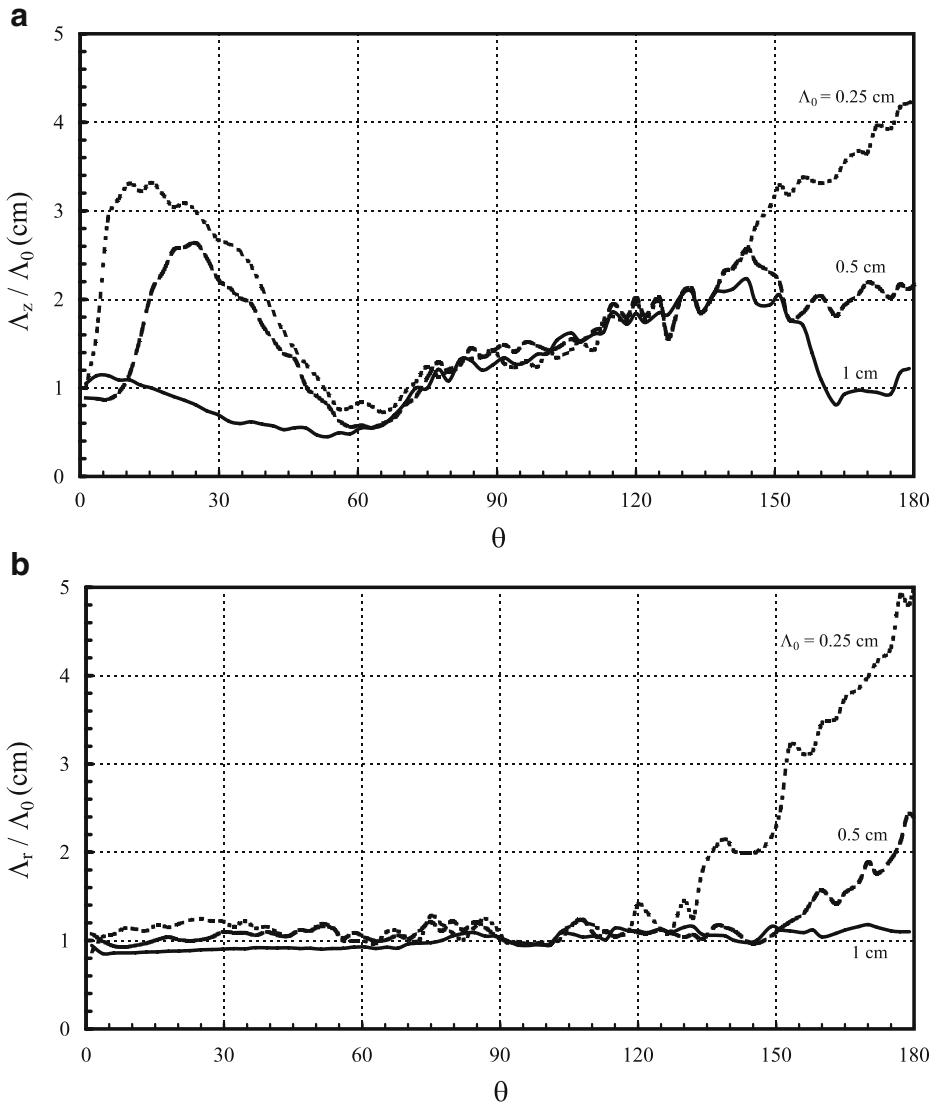

Fig. 10 The integral turbulent length scales in z-direction (**a**) and r-direction (**b**) calculated for the initial lengths $\Lambda_0 = 0.25; 0.5; 1$ (cm) (*dotted*, *dashed* and *solid*, respectively) versus the crank angle θ

pointed above, direct numerical simulations do not allow a sufficiently fine mesh needed to resolve the turbulent length scales as small as created experimentally in Ref. [1]. Still, qualitative comparison of the present numerical results of Fig. 9a and respective experimental data demonstrates a well-pronounced dynamical similarity in the behavior of Λ_z, Λ_r though on different scales. It is interesting to check if the qualitative similarity means also quantitative (self-similar) correlation. For that purpose we compared the experimental results and the numerical ones with proper scaling; comparison is presented in Fig. 9b, c. Since one of the main tasks of the present work was to compare the roles of initial turbulence and piston-generated one, we scaled both our simulations results and experimental data of [1] by the respective initial values. As an alternative, one can take a value averaged over the circle as a scaling factor. Indeed, in Ref. [1] Λ_z decreases from initial values of about 0.7–1 mm to 0.4–0.5 mm close to $\theta = 50^\circ - 60^\circ$, and goes up to 2–2.5 mm at $\theta = 150^\circ$ (measurements stopped at this point). Scaling our simulation results and the experimental data of Ref. [1] by the respective initial values, we observe the same tendency. The last fact suggests self-similar properties of the turbulent flow, independent of any particular initial value of Λ. We point out that present simulations show even somewhat better agreement with experiments than the model studies of Ref. [1]. The agreement obtained demonstrates that the 2D axisymmetric flow studied in the present paper describes the main features of the turbulence of Ref. [1] quite well. In order to verify the self-similar properties of the turbulent flow, we also performed simulations for other initial turbulent length scales. Figure 10 shows integral turbulent length scales in z-direction, Λ_z, (Fig. 10a) and in r-direction, Λ_r, (Fig. 10b) versus the crank angle. The values Λ_z, Λ_r were calculated for the initial lengths $\Lambda_0 = 0.25$; 0.5; 1 (cm) (dotted, dashed and solid lines, respectively). Figure 10a shows three obvious stages in the dynamics of Λ_z. First, we can see relaxation from the artificially chosen initial conditions in the interval $0^\circ < \theta < 60^\circ$; the stage ends up with a local minimum in Λ_z. Then, the turbulent flow develops in a self-similar way independent of any particular initial value of Λ_z. This stage happens in the interval of crank angles $60^\circ < \theta < 150^\circ$; all three plots practically coincide in that case taking into account stochastic nature of the flow. The final, third stage develops close to the TDC, when the piston slows down. At that stage the integral turbulent length scale is determined by the engine geometry, and not by the initial parameters. In all three cases Λ_z approaches 1 cm determined by clearance (scaled by $\Lambda_0 = 0.25$; 0.5; 1 (cm) it leads, of course, to different values in Fig. 10a). Figure 10b shows similar tendency for Λ_r for the same $\Lambda_0 = 0.25$; 0.5; 1 (cm). In that case, all three plots practically coincide in the wide range of angles $0^\circ < \theta < 130^\circ$. Only close to the TDC, at $\theta > 130^\circ$, the scaled plots diverge; but the dimensional values for Λ_r approach 1 cm determined by the engine geometry and independent of initial turbulent parameters.

4 Summary

We performed numerical simulations of a turbulent flow produced by piston motion in a SI engine with a cylindrical chamber. The engine geometry was chosen the same as in the experiments [1]. We considered cases of both zero and non-zero initial turbulence.

In the case of zero initial turbulence, the characteristic values of the turbulent rms-velocity are an order of magnitude smaller than the average piston speed. The integral turbulent length scale is determined by the engine geometry. At the TDC, two large vortex rings of opposite direction dominate in the flow. Both the turbulent intensity and the integral length are larger in the axial direction in comparison with the radial one.

In the other case, we took into account the possibility of initial homogeneous turbulence of large intensity similar to [1]. Different values of initial integral turbulent length were considered. In all cases we observed a typical rms-velocity much smaller than the average piston velocity. It was demonstrated that the turbulent length scale changes in a self-similar way in the wide range of crank angles. However, close to the TDC, the turbulent length scale is determined by the engine geometry, independent of the initial value.

We stress one more time that azimuthal fluctuations and stress component, as well as the tangential vortex stretching remain beyond 2D simulations. For this reason, the present studies give rather qualitative than quantitative comparison to realistic 3D experiments. Meanwhile, they provide the basic qualitative idea about a piston-generated flow in an SI-engine.

Finally, we would like to say few words about possible combustion applications of the present results. One of the popular models of turbulent burning treats a flame front as a passively propagating surface, e.g. see [3, 35–39]. Formally, this model corresponds to "burning" with zero thermal expansion, which does not influence the turbulent flow. Such a model means that turbulence is determined mainly by external sources such as the piston motion studied in the present work. However, evidence is mounting, both experimental and numerical, that flames with realistic thermal expansion modify the initial turbulent flow strongly [10, 40–44]. Recently, we have also performed direct numerical simulations of combustion in a closed burning chamber like a clearance of an SI-engine, see [45]. These simulations demonstrated quite strong influence of burning on the flow even in the case of initial turbulent velocity exceeding the planar flame speed by an order of magnitude. This influence becomes much stronger under confinement than in the opening studied in [8–10]. Current properties of the modified turbulent flow may differ noticeably from the initial ones. Still, even in that case, the initial turbulent intensity and the length scales studied in the present paper remain important parameters controlling total burning time. Basically, there are three factors controlling the flow in SI-engines: (i) turbulence produced during the intake; (ii) turbulence produced by the piston motion; and (iii) flame-generated turbulence. In the present work, we considered and compared first two factors; study of turbulence produced by flame propagation will be presented elsewhere.

Acknowledgements The authors are grateful to Martin Oberlack for the data of paper [1] reproduced in Figs. 8, 9b, c. We also thank Mikhail Modestov for useful discussions. This work has been supported by the Swedish Research Council (VR) and by the Kempe Foundation.

References

1. Breuer, S., Oberlack, M., Peters, N.: Non-isotropic length scales during the compression stroke of a motored piston engine. Flow Turbul. Combust. **74**, 145 (2005)

2. Williams, F.A.: Combustion Theory. Cummings, Menlo Park (1985)
3. Peters, N.: Turbulent Combustion. Cambridge University Press, Cambridge (2000)
4. Poinsot, T., Veynante, D.: Theoretical and Numerical Combustion. Edwards, Ann-Arbor (2005)
5. Lee, T., Lee, S.: Direct comparison of turbulent burning velocity and flame surface properties. Combust. Flame **132**, 492 (2003). doi:10.1016/S0010-2180(02)00495-9
6. Filatiev, S., Driscoll, J., Carter, C., Donbar, J.: Measured properties of turbulent premixed flames. Combust. Flame **141**, 1 (2005). doi:10.1016/j.combustflame.2004.07.010
7. Savarianadam, V., Lawn, C.: Burning velocity of premixed turbulent flames. Combust. Flame 146, 1 (2006). doi:10.1016/j.combustflame.2006.05.002
8. Colin, O., Ducros, F., Veynante, D., Poinsot, T.: A thickened flame model for large Eddy simulations. Phys. Fluids **12**, 1843 (2000). doi:10.1063/1.870436
9. Selle, L., Lartigue, G., Poinsot, T., Koch, R., Schildmacher, K., Krebs, W., Kaufman, Veynante D., et al.: Compressible large Eddy simulation of turbulent combustion in complex geometry of unstructured meshes. Combust. Flame **137**, 489 (2004). doi:10.1016/j.combustflame.2004.03.008
10. Akkerman, V., Bychkov, V., Eriksson, L.E.: Numerical study of turbulent flame velocity. Combust. Flame **151**, 452 (2007). doi:10.1016/j.combustflame.2007.07.002
11. Peters, N., Wenzel, H., Williams, F.A.: Modification of the turbulent burning velocity by gas expansion. Proc. Combust. Inst. **28**, 235 (2000)
12. Bychkov, V.: Importance of the Darrieus–Landau instability for turbulent flames. Phys. Rev. E Stat. Nonlin. Soft Matter Phys. **68**, 066304 (2003). doi:10.1103/PhysRevE.68.066304
13. Akkerman, V., Bychkov, V.: Velocity of weakly turbulent flames of finite thickness. Combust. Theory Model. **9**, 323 (2005). doi:10.1080/13647830500098399
14. Bradley, D., Gaskell, P., Gu, X., Sedaghat, A.: Premixed flamelet modeling. Combust. Flame **143**, 227 (2005). doi:10.1016/j.combustflame.2005.05.014
15. Petchenko, A., Bychkov, V., Eriksson, L.E., Oparin, A.: Flame propagation along the vortex axis. Combust. Theory Model. **10**, 581 (2006). doi:10.1080/13647830600552006
16. Bychkov, V., Petchenko, A., Akkerman, V.: On the theory of turbulent flame velocity. Combust. Sci. Technol. **179**, 137 (2007)
17. Lindborg, E.: Kinematics of homogeneous axisymmetric turbulence. J. Fluid Mech. **302**, 179 (1995). doi:10.1017/S002211209500406X
18. Oberlack, M.: Non-isotropic dissipation in non-homogeneous turbulence. J. Fluid Mech. **350**, 351 (1997). doi:10.1017/S002211209700712X
19. Rouland, E., Trinite, M., Dionnet, F., Flocj, A., Ahmed, A.: Particle Image Velocimetry Measurements in an Engine, SAE 972831 (1997)
20. Hong, C., Tarng, S.: Direct measurement and computational analysis of turbulence length scales of a motored engine. Exp. Therm. Fluid Sci. **16**, 277 (1998). doi:10.1016/S0894-1777(97)10035-8
21. Ramos, J.: Internal Combustion Engine Modeling. Hemisphere, London (1995)
22. Kume, T., Iwamoto, Y., Iida, K., Murakami, M., Akishino, K., Ando, H.: Combustion Control Technologies for SI Engine, SAE 960600 (1996)
23. Zhao, F., Lai, M., Harrington, D.: Automotive spark-ignited direct-injection gasoline engines. Prog. En. Combust. Sci. **25**, 437 (1999). doi:10.1016/S0360-1285(99)00004-0
24. Nikitin, N., Yakhot, A.: Direct numerical simulation of turbulent flow in elliptical ducts. J. Fluid Mech. **532**, 141 (2005). doi:10.1017/S0022112005003964
25. Yap, D., Megaritis, A., Wyszynski, M.: An experimental study of bio-ethanol HCCI. Combust. Sci. Technol. **177**, 2039 (2005)
26. Borman, G., Ragland, K.: Combustion Engineering. McGraw Hill, NY (1988)
27. Hirschfelder, J., Curtiss, C., Bird, R.: Molecular Theory—Gases and Liquids. Wiley, New York (1954)
28. Hilsenrath, J.: Tables of Thermodynamic and Transport Properties. Pergamon, London (1960)
29. Belotserkovsky, O.: Turbulence and Instabilities. Mzpress, Moscow (2003) (in English)
30. Belotserkovsky, O., Oparin, A., Chechetkin, V.: Turbulence: New Approaches. Cambridge Int. Sci. Publishing, Cambridge (2005)
31. Belotserkovsky, O., Davydov, Y.M.: Large-particle Method in Hydrodynamics. Nauka, Moscow (1982) (in Russian)
32. Liberman, M., Ivanov, M., Valiev, D., Eriksson, L.E.: Hot spot formation by the propagating flame and the influence of EGR on knock occurrence in SI engines. Combust. Sci. Technol. **178**, 1613 (2006). doi:10.1080/00102200500536316
33. Landau, L., Lifshitz, E.: Fluid Mechanics. Pergamon, Oxford (1989)

34. Kobayashi, H., Kawazoe, H.: Flame instability effects on the smallest wrinkling scale of high-pressure turbulent premixed flames. Proc. Combust. Inst. **28**, 375 (2000)
35. Clavin, P., Williams, F.A.: Theory of premixed-flame propagation in large-scale turbulence. J. Fluid Mech. **90**, 589 (1979). doi:10.1017/S002211207900241X
36. Kerstein, A.R., Ashurst, W.T., Williams, F.A.: Field equation for interface propagation in an unsteady homogeneous flow field. Phys. Rev. A **37**, 2728 (1988). doi:10.1103/PhysRevA.37.2728
37. Denet, B.: Frankel equation for turbulent flames in the presence of a hydrodynamic instability. Phys. Rev. E Stat. Phys. Plasmas Fluids Relat. Interdiscip. Topics **55**, 6911 (1997). doi:10.1103/PhysRevE.55.6911
38. Kagan, L., Sivashinsky, G.: Flame propagation and extinction in large-scale vortical flows. Combust. Flame **120**, 222 (2000). doi:10.1016/S0010-2180(99)00090-5
39. Bychkov, V., Denet, B.: Effect of temporal pulsations of a turbulent flow on the flame velocity. Combust. Theory Model. **6**, 209 (2002). doi:10.1088/1364-7830/6/2/304
40. Chen, Y.C., Bilger, R.: Experimental investigation of three-dimensional flame front structure in premixed turbulent combustion. Combust. Flame **131**, 400 (2002). doi:10.1016/S0010-2180(02)00418-2
41. Swaminathan, N., Bray, K.: Effect of dilatation on scalar dissipation in turbulent premixed flames. Combust. Flame **143**, 549 (2005). doi:10.1016/j.combustflame.2005.08.020
42. Swaminathan, N., Grout, R.: Interaction of turbulence and scalar fields in premixed flames. Phys. Fluids **18**, 045102 (2006). doi:10.1063/1.2186590
43. Chakraborty, N., Swaminathan, N.: Influence of the damkohler number on turbulence-scalar interaction in premixed flames I. Phys. Fluids **19**, 045103 (2007). doi:10.1063/1.2714070
44. Chakraborty, N., Swaminathan, N.: Influence of the damkohler number on turbulence-scalar interaction in premixed flames II. Phys. Fluids **19**, 045104 (2007). doi:10.1063/1.2714076
45. Akkerman, V., Bychkov, V., de Goey, L., Bastiaans, R., van Oijen, J., Eriksson, L.-E.: Flow-flame interaction in a closed chamber. Phys. Fluids **20**, 055107 (2008). doi:10.1063/1.2919807